Single-loop-like energy oscillations and staircase vortex occupation in superconducting double networks

I. Sochnikov,[1] Y. Shokef,[2] A. Shaulov,[1] and Y. Yeshurun[1]

[1]*Department of Physics, Institute of Superconductivity and Institute of Nanotechnology and Advanced Materials, Bar-Ilan University, Ramat-Gan 52900, Israel*

[2]*Department of Materials and Interfaces, Weizmann Institute of Science, Rehovot 76100, Israel*

(Received 22 December 2010; published 12 July 2011)

The magnetic-field dependence of the energy and vortex occupation is calculated for the recently realized superconducting double network consisting of two interlaced subnetworks of small and large loops. Two different approaches are employed, both based on the J^2 model: Mean-field analysis that minimizes the network energy assuming random-vortex configurations and numerical simulations in which energy is minimized avoiding this assumption. In the mean-field analysis the vortex population in both subnetworks increases linearly with the applied field. In contrast the simulations show that while the population of the large loops increases linearly with field, the occupation of the small loops grows in steps, resembling the behavior of an ensemble of decoupled loops. This decoupling is also reflected in the waveform of the energy versus applied field. A modified mean-field analysis, which introduces decoupling between the small loops, yields results in excellent agreement with the simulations. These findings suggest that the behavior of a single loop is reflected in the double network and thus constitute it as a favorable system for the experimental study of quantization effects in superconducting loops.

DOI: 10.1103/PhysRevB.84.024513 PACS number(s): 74.81.Fa, 74.78.Na, 74.25.Uv, 75.75.−c

I. INTRODUCTION

In the early days of superconductivity London predicted that the fluxoid,[1] defined as the sum of the magnetic flux and a term involving the persistent current, is quantized in a multiply connected superconductor in units of $\phi_0 = hc/2e$. For a single superconducting loop the fluxoid quantization, together with the requirement for energy minimization, dictates periodic changes in the screening current density J and step-wise occupation of the loop with flux quanta. The energy, being proportional to J^2, is also periodic with the magnetic field, giving rise to periodic changes in the critical temperature T_c as demonstrated by Little and Parks.[2]

Similar to a single superconducting loop, two-dimensional periodic networks of superconducting loops also exhibit magnetoresistance oscillations with field periodicity ϕ_0/A, where A corresponds to the area of each loop in the network.[3–11] Analyses of the current distribution and the energy versus magnetic field in such networks is usually based on the J^2 model[12–14] assuming current conservation in each node and that the average field for the entire network is equal to the externally applied field.[15–17]

Recently, we fabricated a novel type of superconducting network[18,19] made by connecting the vertexes of small square loops with relatively long wires, forming two interlaced subnetworks of small and large loops, see Fig. 1(a). The motivation for designing such a network was to create an array of decoupled small loops that behave like isolated loops. Here we analyze this unique network employing two theoretical approaches both based on the J^2 model. The first is the mean-field approach that minimizes the network energy assuming random vortex configurations, and the second is based on numerical simulations in which energy is minimized avoiding this assumption. We first demonstrate these two approaches in the analysis of a *simple square lattice* [Fig. 1(b)]. Although in this case both methods yield similar results for the periodicity and the occupation rate, the numerical simulations show additional local minima at normalized fields $0.5 + m$, with integer m corresponding to the checkerboard configuration studied previously.[3,12,14,20] More dramatic differences between the two approaches are manifested in the analysis of the *double network* [Fig. 1(a)]. While in the naïve mean-field analysis the vortex population in both sublattices of small and large loops increases linearly with the applied field, the numerical simulations show that the occupation of the small loops grows in steps, resembling the behavior of an ensemble of nearly decoupled loops. However, we show that a modified mean-field analysis which includes decoupling between the small loops reproduces the staircase-vortex occupation and the energy waveform obtained in the simulations. Finally we point to the advantage of the numerical simulations in providing the actual spatial distribution of the vortices in the double network, demonstrating visually the different occupation of the large and small loops at various magnetic fields. These results will guide future experimental efforts to measure vortex occupations in such complex networks.

II. SQUARE NETWORK

We consider a network of $M \times M$ square loops, each of side L, in an external magnetic field H [see Fig. 1(b)]. The fluxoid quantization[1,21] requires that the integral over the currents around each loop is balanced by the flux quanta in the loop and the external magnetic flux. Thus,

$$\sum_{\delta} L J_{\delta\alpha} = N_\alpha \phi_0 - H L^2, \tag{1}$$

where $\delta = 0,1,2,3$ indexes the edges of the square loop $\alpha = 0,1 \ldots M^2 - 1$, carrying a screening current $J_{\delta\alpha}$, and N_α is the number of vortices in the loop α.

 ©2011 American Physical Society

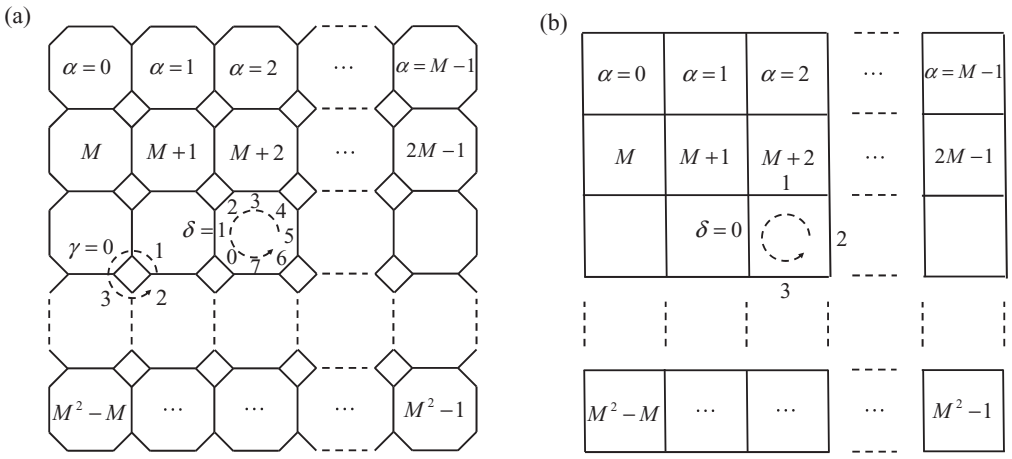

FIG. 1. Schematic diagram of (a) the double network and (b) the simple square network.

The energy is given by the sum of J^2 over all the network wires,

$$E = \sum_{\alpha=0}^{M^2-1} L\left(J_{0\alpha}^2 + J_{1\alpha}^2\right), \tag{2}$$

where two sides in each loop are considered, and the summation over all loops ensures that each wire in the network is accounted for. Equations (1) and (2) are the basis for both the mean field and the numerical-simulation approaches. In writing these equations we adopted the assumptions of the J^2 model,[12–14] namely that the magnetic-penetration length is much larger than wires' width and the screening currents are therefore very small. These currents produce magnetic fields that are perturbations on the applied field and are therefore neglected. This model also neglects the geometric inductance[22,23] and the additional energy from the induced currents interacting with the applied field as compared to the kinetic energy. Notably, the model assumption on the screening length is well satisfied in our experiments.[18,19]

A. Mean-field solution

We assume that a fraction F of the square loops have $N+1$ vortices and the remaining $1-F$ have N. Therefore the total magnetic flux through the system is

$$N_T[F(N+1)+(1-F)N]\phi_0 = HN_TL^2, \tag{3}$$

where $N_T = M^2$ is the number of loops in the lattice. Thus

$$N + F = \frac{HL^2}{\phi_0}. \tag{4}$$

Because F is a fraction and N is an integer, we may write

$$F = \left\{\frac{HL^2}{\phi_0}\right\}, \quad N = \left|\frac{HL^2}{\phi_0}\right|, \tag{5}$$

where $\{\bullet\}$ denotes the fractional part and $|\bullet|$ the integer part.

We refer to a loop-carrying $(N+1)$ flux quanta as occupied and to one carrying only N quanta as vacant. Each edge in the network has two neighboring loops, and in the mean-field approximation the probability that both loops are occupied is F^2, that one is occupied and one is vacant $2F(1-F)$, and that both are vacant is $(1-F)^2$. Moreover, we will assume that these three types of edges carry currents J_{++}, J_{+-}, and J_{--}, respectively. Hence, the average current in the system is

$$\langle J\rangle = F^2J_{++} + 2F(1-F)J_{+-} + (1-F)^2J_{--}. \tag{6}$$

Equation (1) for the occupied and vacant loops takes the form

$$\begin{aligned} 4L[FJ_{++}+(1-F)J_{+-}] &= (N+1)\phi_0 - HL^2 = (1-F)\phi_0 \\ 4L[FJ_{+-}+(1-F)J_{--}] &= N\phi_0 - HL^2 = -F\phi_0. \end{aligned} \tag{7}$$

In writing Eq. (7), we assumed that for each one of the four loops surrounding a given loop, there is a probability F to be occupied and probability $1-F$ to be vacant. It is straightforward to verify from Eqs. (6) and (7) that the requirement that the average current in the network $\langle J\rangle = 0$ is automatically satisfied.

Equation (2), for the energy, takes the form

$$E = 2N_TL[F^2J_{++}^2 + 2F(1-F)J_{+-}^2 + (1-F)^2J_{--}^2]. \tag{8}$$

We are interested in the minimal energy for a given external field; therefore, we seek the current distribution in the system that minimizes the energy given in Eq. (8). We use the constraints of Eq. (7) to express J_{++} and J_{--} in terms of J_{+-}, then substitute these in Eq. (8) and minimize with respect to J_{+-} by requiring $\partial E/\partial J_{+-} = 0$. After some algebra this yields

$$E = \frac{N_T\phi_0^2}{4L}F(1-F). \tag{9}$$

The solid line in Fig. 2 shows the normalized energy per loop as a function of the normalized external field. Note that the energy waveform for the network is inverted and shifted by a quarter of a period relative to that of a single loop (see, e.g., Fig. 4.5[21]). In addition, in contrast to an isolated loop in which the occupation grows in steps,[21] in the square network the occupation grows linearly with the field, see Eq. (4).

This solution is valid as long as the vortex distribution in the network is disordered, namely that there are no correlations between the occupations of neighboring loops. It is instructive to see how this breaks down for $F = 1/2$, where

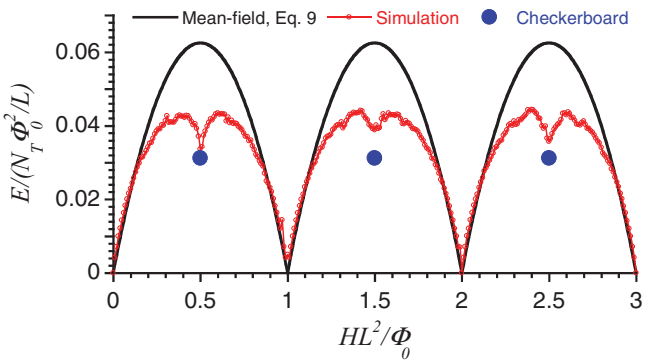

FIG. 2. (Color online) Normalized energy per loop obtained from the mean-field analysis [Eq. (9)] and from the simulations (solid line and open circles, respectively) plotted versus the normalized field. The bold circles indicate the theoretical value of the energy corresponding to the checkerboard configuration of vortices in the square network $E = N_T\phi_0^2/(32L)$.

the minimum energy configuration is known to be that of a checkerboard arrangement of the vortices on the lattice. For such a configuration, all edges have an occupied loop on one side and a vacant loop on the other.[24,25] Equation (7) should be modified to have only contributions from J_{+-} for both types of loops, which leads to $J_{+-} = \phi_0^2/(8L)$. Similarly, Eq. (8) for the energy should be modified to include only a contribution from J_{+-}^2, eventually leading to $E = N_T\phi_0^2/(32L)$, denoted by the bold circles in Fig. 2, which is half of the mean-field value of $N_T\phi_0^2/(16L)$ obtained by substituting $F = 1/2$ in Eq. (9). Also note that for the checkerboard arrangement of vortices, Eq. (6) may no longer be used, yet the total current still vanishes. Here the magnitude of the current on all edges is equal, but their directions alternate in space to achieve a net current in one direction around the occupied loops and in the opposite direction around the vacant loops.

The numerical simulation, discussed in the next section, offers a more accurate solution, not limited to disordered distributions of vortices in the network.

B. Numerical simulation

For a given external field H we calculate the total number of vortices in the system as

$$N_V = N_T L^2 H/\phi_0. \tag{10}$$

We initially distribute these vortices randomly throughout the network. Then we employ the following procedure to find the currents $J_{\delta\alpha}$ through all edges such that the total energy of the network is minimized: We assign a circular current $\tilde{J}_\beta$ to each loop β and express $J_{\delta\alpha}$ in terms of $\tilde{J}_\beta$,

$$J_{\delta\alpha} = \sum_\beta K^\delta_{\alpha\beta}\tilde{J}_\beta, \tag{11}$$

where the four $N_T \times N_T$ matrices K^0,K^1,K^2, and K^3 are evaluated in Appendix A, assuming current conservation at every node of the network[26] and periodic-boundary conditions. Equation (11) provides four sets of M^2-linear equations. By substituting Eq. (11) into Eq. (1), one gets N_T-linear equations with M^2 variables $\tilde{J}_\beta$,

$$N_\alpha\phi_0 - HL^2 = \sum_{\delta\beta} LK^\delta_{\alpha\beta}\tilde{J}_\beta = \sum_\beta \Upsilon_{\alpha\beta}\tilde{J}_\beta. \tag{12}$$

where $\Upsilon_{\alpha\beta} = \sum_\delta LK^\delta_{\alpha\beta}$ is an $M^2 \times M^2$ matrix. Having the population vector $\mathbf{N}$ we evaluate the vector of the circular currents $\tilde{\mathbf{J}}$ by inversion

$$\tilde{\mathbf{J}} = \mathbf{Y}^{-1}(\mathbf{N}\phi_0 - HL^2). \tag{13}$$

Knowledge of $\tilde{\mathbf{J}}$ for a given spatial distribution of the vortices on the lattice allows calculation of the current matrix $J_{\delta\alpha}$ using Eq. (11) and thus the total energy E using Eq. (2).

The minimum energy and the vortex configuration corresponding to it are found as follows: One cell is randomly chosen and the number of vortices in this cell is reduced by one, and subsequently the number of vortices in one of the neighboring cells is incremented by one. We calculate the currents $J_{\delta\alpha}$ and the energy for the new configuration. If the energy of this new configuration is lower than the energy of the previous state, then we accept the new one. Otherwise the old state is preserved. This process is repeated for every cell in the network, completing one sweep of energy minimization. Such sweeps are repeated (typically 500–1000 times) until we reach a steady state. Results of the calculated energy for a 10×10 network are shown in Fig. 2 (open circles). Convergence of the calculations presented in Fig. 2 was confirmed for several fields in a 20×20 network.

Notably, although the periodicity of the energy versus field and the occupation rate are as in the mean-field case, the simulation shows local minima at normalized fields $1/2 + m$, with integer m corresponding to the checkerboard configuration.[3,12,14,24,25] Hints for additional minima at normalized magnetic fields of $1/3$ and $2/3$ may be observed in Fig. 2 in agreement with, e.g., Pannetier *et al.*[9] Additional possible minima are in the noise level. More dramatic differences between the two approaches of the mean-field solution and numerical simulations are found in the case of the double network, as described in subsequent sections.

III. DOUBLE NETWORK

We refer to the double network of Fig. 1(a) made up of a square lattice of side L and square loops of side $\ell < L$ oriented at 45° with respect to this lattice and placed at every vertex of the large lattice. Each large loop has four short edges of length ℓ and four long edges of length $x = L - \sqrt{2}\ell$. (We refer to these edges as long even though for $x < \ell$, $\sqrt{2}\ell < L < (1+\sqrt{2})\ell$.) The area of each small loop is ℓ^2, and the area of each large loop is $L^2 - \ell^2$.

A. Mean-field solution

When this system is placed in an external magnetic field H, a fraction f of the small loops have $n+1$ flux quanta through them, and a fraction $1-f$ have n, and similarly, a fraction F of the large loops have $N+1$, and a fraction $1-F$ have N.

These quantities are related to the external field since the total magnetic flux satisfies

$$N_T[f(n+1)+(1-f)n+F(N+1)+(1-F)N]\phi_0 = HN_TL^2. \tag{14}$$

The left-hand side is the result of counting the number of flux quanta according to the above definitions (N_T is the number of loops of each size), and the right-hand side is the external field multiplied by the total area of the system. This leads to

$$N+F+n+f=\frac{HL^2}{\phi_0}. \tag{15}$$

In deriving the mean-field solution for the double grid, we note that as for the simple square lattice, there are three types of long edges: those separating two occupied loops (++), those separating an occupied loop and a vacant loop (+−), and those separating two vacant loops (−−). We assume that the probabilities of finding each of these types are given by F^2, $2F(1-F)$, and $(1-F)^2$, respectively. We assume these types of edges carry currents J_{++}, J_{+-}, and J_{--}, respectively. Therefore, the requirement that the average current vanishes[26] reads

$$\langle J\rangle = F^2J_{++}+2F(1-F)J_{+-}+(1-F)^2J_{--}=0. \tag{16}$$

Each short edge separates a small loop and a large loop, therefore the types (+−) and (−+) are not symmetric as for the long edges, and we need to deal with four types of edges: separating two occupied loops (++), separating an occupied small loop and a vacant large loop (+−), separating a vacant small loop and an occupied large loop (−+), and separating two vacant loops (−−). We assume currents j_{++}, j_{+-}, j_{-+}, and j_{--} on them, and within the mean-field approximation, the probabilities of finding each of them are given by fF, $f(1-F)$, $(1-f)F$, and $(1-f)(1-F)$, respectively. The requirement that the average current on the short edges vanishes is

$$\langle j\rangle = fFj_{++}+f(1-F)j_{+-}+(1-f)Fj_{-+} +(1-f)(1-F)j_{--}=0. \tag{17}$$

An occupied small loop has the following relation between the integral of the currents around it and the magnetic flux through it,

$$4\ell[Fj_{++}+(1-F)j_{+-}]=(n+1)\phi_0-H\ell^2. \tag{18}$$

For a vacant small loop we similarly have

$$4\ell[Fj_{-+}+(1-F)j_{--}]=n\phi_0-H\ell^2. \tag{19}$$

The currents on each of the edges are determined by the flux in the large loop on the other side of that edge, and we have used the mean-field assumption that the flux in adjacent loops is uncorrelated, thus the probabilities for having each of the neighboring large loops occupied or vacant are F and $1-F$, respectively.

Similarly, an occupied large loop has

$$4\ell[fj_{++}+(1-f)j_{-+}]+4x[FJ_{++}+(1-F)J_{+-}] =(N+1)\phi_0-H(L^2-\ell^2), \tag{20}$$

and a vacant large loop has

$$4\ell[fj_{++}+(1-f)j_{-+}]+4x[FJ_{++}+(1-F)J_{+-}] =N\phi_0-H(L^2-\ell^2). \tag{21}$$

Multiplying Eq. (18) by F and Eq. (19) by $1-F$ and then adding leads, by the use of Eq. (17), to

$$\frac{n+f}{N+F}=\frac{\ell^2}{L^2-\ell^2}. \tag{22}$$

It is easy to see that now Eq. (16) is satisfied as well. Together with Eq. (15), we obtain $N+F=H(L^2-\ell^2)/\phi_0$ and $n+f=H\ell^2/\phi_0$. Because N and n should be integer and f and F fractional, we obtain

$$F=\left\{\frac{H(L^2-\ell^2)}{\phi_0}\right\},\quad N=\left|\frac{H(L^2-\ell^2)}{\phi_0}\right|, \qquad f=\left\{\frac{H\ell^2}{\phi_0}\right\},\quad n=\left|\frac{H\ell^2}{\phi_0}\right|, \tag{23}$$

where $\{\bullet\}$ denotes the fractional part and $|\bullet|$ the integer part.

We are now left with four Eqs. (18)–(21), connecting the seven unknown currents (J_{++}, J_{+-}, J_{--}, j_{++}, j_{+-}, j_{-+}, j_{--}). We use these four equations to express J_{++}, J_{--}, j_{++}, and j_{--} in terms of J_{+-}, j_{+-}, and j_{-+}. The energy, given by the sum of xJ^2 over $2N_T$ long edges and the sum of ℓj^2 over $4N_T$ short edges,

$$E=2N_Tx[F^2J_{++}^2+2F(1-F)J_{+-}^2+(1-F)^2J_{--}^2] +4N_T\ell[fFj_{++}^2+f(1-F)j_{+-}^2+(1-f)Fj_{-+}^2 +(1-f)(1-F)j_{--}^2] \tag{24}$$

may now be expressed in terms of the parameters J_{+-}, j_{+-}, and j_{-+}. We minimize E with respect to these parameters by demanding that $\partial E/\partial J_{+-}=\partial E/\partial j_{+-}=\partial E/\partial j_{-+}=0$. After some algebra, this yields

$$E=\frac{N_T\phi_0^2}{4}\left[\frac{F(1-F)}{x+\ell}+\frac{f(1-f)}{\ell}\right]. \tag{25}$$

Figure 3(a) and 3(b) show the mean-field calculations [Eq. (25)] of the normalized energy per unit-cell of the double network and the occupation $N_v=N+F$ and $n_v=n+f$ of the large and the small loops, respectively, for $L/\ell=5$. The short period oscillations shown in Fig. 3(a) are associated with the large loops. These oscillations are superimposed on oscillations of longer periods associated with the small loops. Figure 3(b) shows that the mean-field solution predicts that the occupation of both the large and small loops increases linearly with the field, behaving as in two separate square networks consisting of large and small loops. As described in the following section, the numerical simulations show that while the occupation of the large loops increases roughly linearly with the applied field, the occupation of the small

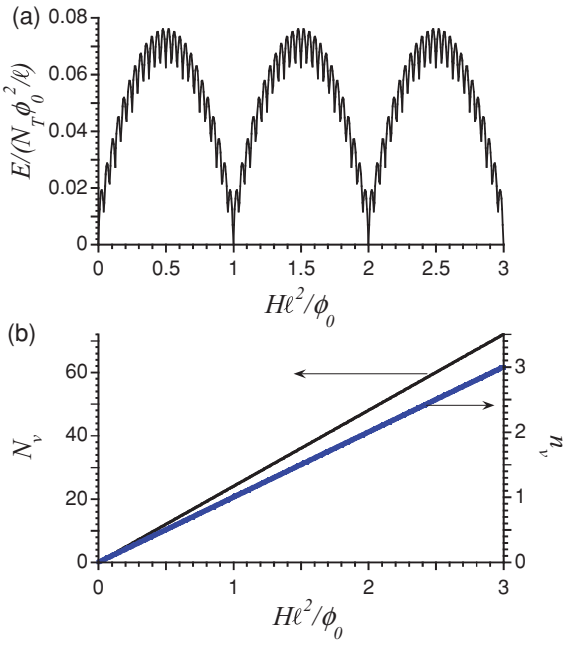

FIG. 3. (Color online) (a) Mean-field calculations [Eq. (25)] of the normalized energy per unit-cell of the double network, and (b) the occupation $N_v = N + F$ of large and small loops $n_v = n + f$ for $L/\ell = 5$. Note that the ratio of the slopes of the two lines is 24, which corresponds to the ratio between the areas of the large and small loops.

loops grows in steps, resembling the behavior of an ensemble of nearly decoupled loops.

B. Numerical simulations

For the *double network* [Fig. 1(a)] the fluxoid quantization takes a form of two systems of discrete sums

$$\begin{aligned}\sum_{\delta} L_\delta J_{\delta\alpha} &= N_\alpha\phi_0 - H(L^2-\ell^2)\\ \sum_{\gamma} \ell j_{\gamma\alpha'} &= n_{\alpha'}\phi_0 - H\ell^2.\end{aligned} \tag{26}$$

where $J_{\delta\alpha}$ is the current through the side $\delta = 0,1\ldots7$ of the loop α in the subnetwork of the large loops, and $j_{\gamma\alpha}$ is the current through the side $\gamma = 0,1\ldots3$ of the small loop $\alpha\prime$ adjacent to the large loop α [see Fig. 1(a)]. $L_\delta = x$ for $\delta =$ 1,3,5,7, and $L_\delta = \ell$ for $\delta = 0,2,4,6$. Thus we have N_T-linear equations for the population of vortices in the large loops, and N_T equations for the vortices in the small loops. As for the simple network, we rather use the notation of circular currents: $\tilde{J}$ for large loops and $\tilde{j}$ for small loops. The total current in a specific wire is then expressed using these circular currents:

$$\begin{aligned}J_{\delta\alpha} &= \sum_{\beta} A^{\delta}_{\alpha\beta}\tilde{J}_\beta + \sum_{\beta} B^{\delta}_{\alpha\beta}\tilde{j}_\beta\\ j_{\gamma\alpha} &= \sum_{\gamma\beta} C^{\gamma}_{\alpha\beta}\tilde{J}_\beta + \sum_{\gamma\beta} D^{\gamma}_{\alpha\beta}\tilde{j}_\beta,\end{aligned} \tag{27}$$

where the $N_T \times N_T$ matrices A^δ,B^δ,C^γ, and D^γ are evaluated in Appendix B, assuming current conservation at every node of the network[26] and periodic boundary conditions. Substitution of the total currents from Eq. (27) to Eq. (26) leads to the quantization rule expressed in terms of the circular currents

$$\begin{aligned}\sum_{\delta\beta} L^\delta A^{\delta}_{\alpha\beta}\tilde{J}_\beta + \sum_{\delta\beta'} L^\delta B^{\delta}_{\alpha\beta'}\tilde{j}_{\beta'} &= \sum_{\beta} Y^{(0)}_{\alpha\beta}\tilde{J}_\beta + \sum_{\beta'} Y^{(1)}_{\alpha\beta'}\tilde{j}_{\beta'}\\ &= N_\alpha\phi_0 - H(L^2-\ell^2)\\ \sum_{\gamma\beta} \ell C^{\gamma}_{\alpha'\beta}\tilde{J}_\beta + \sum_{\gamma\beta'} \ell D^{\gamma}_{\alpha'\beta'}\tilde{j}_{\beta'} &= \sum_{\beta} Y^{(2)}_{\alpha'\beta}\tilde{J}_\beta + \sum_{\beta'} Y^{(3)}_{\alpha'\beta'}\tilde{j}_{\beta'}\\ &= n_{\alpha'}\phi_0 - H\ell^2.\end{aligned} \tag{28}$$

Using vector form we can invert Eq. (28) and derive the vectors of circular currents $\tilde{\mathbf{J}}$ and $\tilde{\mathbf{j}}$

$$\begin{bmatrix}\tilde{\mathbf{J}}\\ \tilde{\mathbf{j}}\end{bmatrix} = \begin{bmatrix}\mathbf{Y}^{(0)} & \mathbf{Y}^{(1)}\\ \mathbf{Y}^{(2)} & \mathbf{Y}^{(3)}\end{bmatrix}^{-1}\begin{bmatrix}\mathbf{N}\phi_0 - H(L^2-\ell^2)\\ \mathbf{n}\phi_0 - H\ell^2\end{bmatrix}, \tag{29}$$

where $\mathbf{Y}^{(0)}$, $\mathbf{Y}^{(1)}$, $\mathbf{Y}^{(2)}$, and $\mathbf{Y}^{(3)}$ are $N_T \times N_T$ submatrices, $\mathbf{N}$ and $\mathbf{n}$ are the number of vortices in the large and the small loops, respectively, written in vector form.

The energy of the network is expressed in terms of the currents in each wire:

$$E = \sum_{\substack{\alpha\\ \delta=0,1,2,3,4,6}} L_\delta J^2_{\delta\alpha}, \tag{30}$$

by summing over α we ensure that each of the sides, including $\delta = 5,7$, are accounted for.

As described in Sec. I, the algorithm is based on minimizing the energy associated with the kinetic energy of the screening currents induced in the superconducting network. For the double network the occupation is described by a vector of length $2N_T$, corresponding to N_T small and N_T large loops. For a given external field H, at the initial step the loops are randomly filled with $N_T HL^2/\phi_0$ vortices. Using Eqs. (27) and (29), we calculate the currents induced in the sides of the small and large loops. Knowledge of these currents allows the calculation of the energy of the network using Eq. (30).

The minimum energy of the double network and the vortex configuration corresponding to it are found following a similar procedure as described previously. Namely one cell, small or large, is randomly chosen and one vortex is moved from this cell to one of its nearest neighbors, and the currents $J_{\delta\alpha}$ and $j_{\gamma\alpha}$, and the energy for the new configuration, are calculated. If the energy of this new configuration is lower than the energy of the previous state, then we accept the new one. Otherwise the old state is preserved. We repeat this procedure for every cell in the network (i.e., $2N_T$ times), completing one sweep of the energy minimization. Such sweeps are repeated (typically 500–1000 times). The symbols in Fig. 4 present the results of these calculations for a network consisting of 10×10 large and 10×10 small loops for different values of the ratio L/ℓ. Numerical convergence of the calculations was confirmed for several fields in a 20×20 network of $L/\ell = 5$.

The squares in Fig. 4(a) show the normalized energy of the double network for $L/\ell = 10$, 5, and 3. As in the mean-field solution, oscillations of short periods, corresponding to the large loops, are superimposed on the oscillations of large periods corresponding to the small loops. However, we note that the waveform of the large-period oscillations resemble that

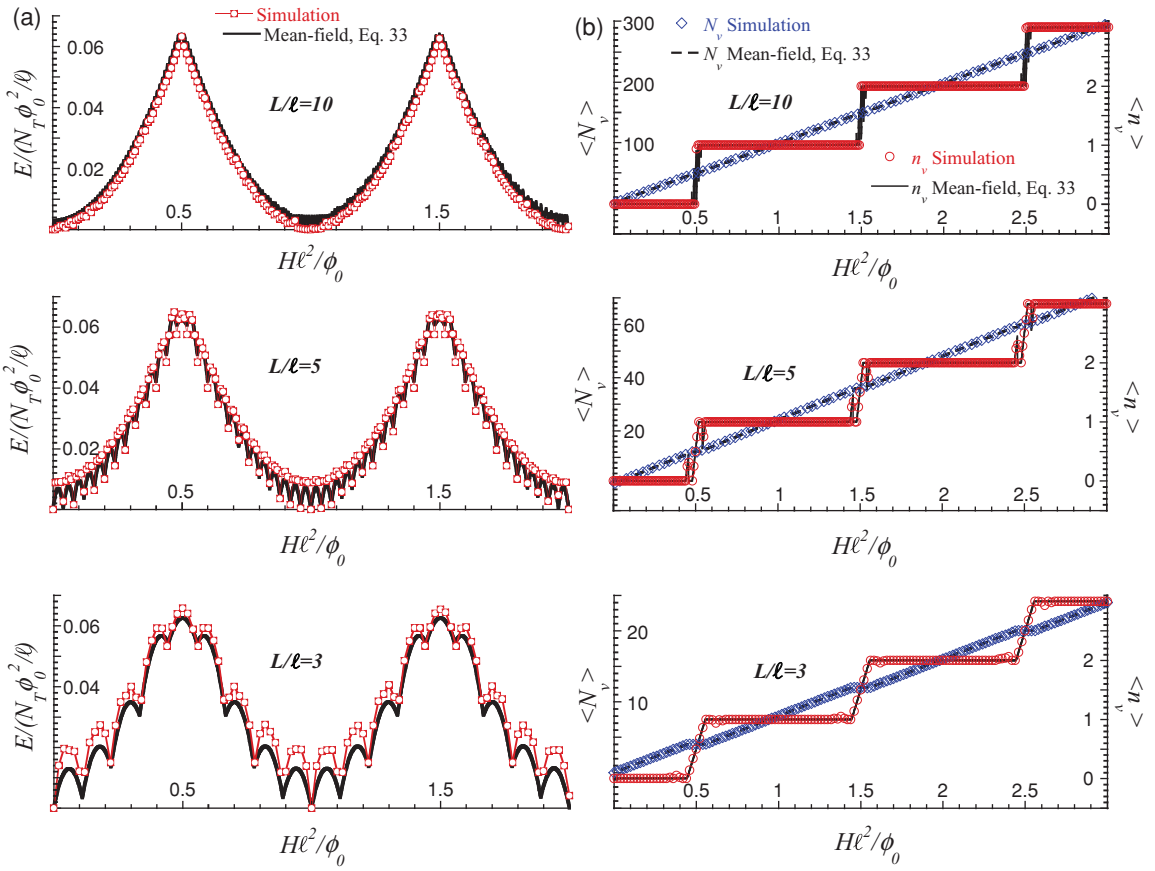

FIG. 4. (Color online) (a) Normalized energy per unit-cell obtained theoretically after minimizing Eq. (33) (bold solid lines) and from simulations (squares connected by thin lines as guide for the eye). (b) Average number of vortices per large loop $\langle N_v\rangle$ and per small loop $\langle n_v\rangle$ obtained theoretically [Eq. (33)] (dashed and solid lines, respectively) and from simulations (diamonds and circles, respectively). The different panels relate to double networks with size ratios $L/\ell = 10$, 5, and 3 (from top to bottom). Both numerical and analytical solutions show breaks around the middle of the steps resulting from competition in occupation of large and small loops. This competition occurs in the field range where the energy cost to insert a vortex into a small loop or a large loop is similar. The field increment (in units of $H\ell^2/\phi_0$) in the simulations is 0.02 for $L/\ell = 3$ and 0.01 for $L/\ell = 5$ and 10. The step in the $\langle n_v\rangle$ plot for $L/\ell = 10$ is relatively sharp (<0.01) and hence points on this step are absent.

of a single loop (i.e., minima at integer multiples of flux quanta and cusps at integer multiples of half-flux quanta) in contrast with the results of the mean-field solution [Fig. 3(a)], which exhibits a waveform similar to the simple square network shown in Fig. 2.

The diamonds and circles in Fig. 4(b) show the average number of vortices per loop calculated for the large and small loops, respectively, as a function of the magnetic flux normalized to the area of the small loops. Results are shown for three ratios $L/\ell = 3,5,10$. The large loops are filled with vortices approximately linearly as the magnetic field increases. In contrast, the small loops are filled in a step-wise manner that becomes sharper as the ratio L/ℓ increases. This indicates that the system prefers to distribute vortices between the large loops and to expel vortices from the small loops. Only when the normalized magnetic field is close to $0.5 + m$, the system may accept vortices into the small loops. This behavior is not predicted in the framework of the mean-field solution as described in the previous section. The step-wise occupation and the energy waveform both imply that the sublattice of the small loops behaves as an ensemble of decoupled single loops.[27] In the next section we show how these results may be obtained theoretically from a modified mean-field model, assuming decoupling of the small loops.

C. Modified mean-field model

As mentioned previously, the mean-field analysis of the double network described in Sec. IIA shows that the two sublattices of the double network are populated as two separate square lattices. This is in contrast with the results of the simulations presented in Sec. IIB that show stepwise occupation of the small loops. We will now show how an assumption on the decoupling between the small loops may be introduced into the mean-field description, and that this hybrid framework explains the numerical findings. We incorporate the decoupling of the small loops by ignoring the requirement that the currents around them should match with the currents on their neighboring large loops. Namely, for the large loops we assume the square-lattice mean-field description with Eq. (7) replaced by:

$$\begin{aligned} \beta_L[F J_{++} + (1-F)J_{+-}] &= (N+1)\phi_0 - \alpha_L H \\ \beta_L[F J_{+-} + (1-F)J_{--}] &= N\phi_0 - \alpha_L H. \end{aligned} \tag{31}$$

Here, the total area $N_T L^2$ is covered by a square lattice of N_T large loops, each with area $\alpha_L = L^2 - \ell^2$ and perimeter $\beta_L = 4(x + \ell) = 4(L + (1 - \sqrt{2})\ell)$, and with N_T disconnected small loops, each with area $\alpha_S = \ell^2$ and perimeter $\beta_S = 4\ell$. We use the convention N, F, n, and f from Sec. IIA to describe the population of these loops, and as in the mean-field solution, compliance of the total magnetic flux with the external field leads to Eq. (15).

For each small loop we assume that the current is distributed uniformly around its perimeter; for a small loop carrying k vortices, this current is thus $j = (k\phi_0 - \alpha_s H)/\beta_s$, resulting in an energy $E = j^2\beta_S = (k\phi_0 - \alpha_s H)^2/\beta_s$. From Eq. (31) we express J_{++} and J_{--} in terms of J_{+-} and substitute the result in the expression for the energy:

$$\frac{E}{N_T} = \frac{\beta_L}{4}[F^2 J_{++}^2 + 2F(1-F)J_{+-}^2 + (1-F)^2 J_{--}^2] + \\ + \frac{f}{\beta_S}[(n+1)\phi_0 - \alpha_S H]^2 + \frac{1-f}{\beta_S}[n\phi_0 - \alpha_S H]^2, \tag{32}$$

where the first term is the mean-field expression for the contribution to the energy from the large loops [see Eq. (8)], and the last two terms average the contributions from populated and vacant small loops according to their abundance. By minimizing E with respect to J_{+-} we eventually obtain

$$\frac{E}{N_T} = \frac{[(N+F)\phi_0 - \alpha_L H]^2 + 2F(1-F)\phi_0^2}{4\beta_L} \\ + \frac{[(n+f)\phi_0 - \alpha_S H]^2 + f(1-f)\phi_0^2}{\beta_S}. \tag{33}$$

Note that we are still free to choose the ratio $(N + F)/(n + f)$ such that Eq. (33) is minimized.

The bold solid lines in Fig. 4(a) show the normalized energy per unit-cell obtained after minimizing Eq. (33) for $L/\ell = 10$, 5, and 3 (from top to bottom). Impressive agreement with the results of the simulations [circles in Fig. 4(a)] is evident. The dashed and solid lines in Fig. 4(b) show the average number of vortices per large loop N_v and per small loop n_v, respectively, as calculated from Eq. (33). These results are in perfect agreement with the results of the simulations described by diamonds and circles in Fig. 4(b). Note that our hybrid model treats the large loops by mean-field interactions and the small loops as disconnected. Yet the behavior of the small loops is not identical to that of loops without network, since the presence of the large loops affects the distribution of vortices in the small ones. For example, as shown in Fig. 4(b), for small L/ℓ the steps in n_v are not sharp as expected for loops without network. These steps become sharper as the ratio L/ℓ increases.

D. Spatial configuration of vortices

Our numerical simulation allows mapping the occupation of the small and large loops in the double network in the state of minimum energy for different external fields. Figure 5 shows the distribution of vortices in a double network with $L/\ell = 5$ at low normalized fields. In this field range the large loops are occupied in the same way as a simple square network: For

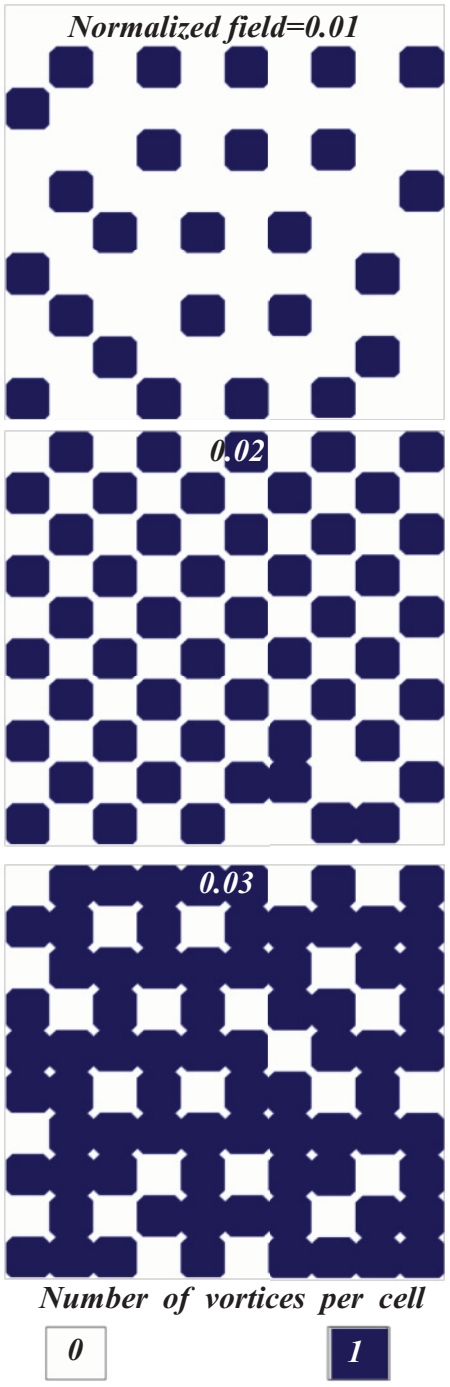

FIG. 5. (Color online) Vortex configuration in the double network at low normalized fields, $H\ell^2/\phi_0 = 0.01, 0.02$ and 0.03 for $L/\ell = 5$. The large loops are continuously occupied in the same way as in a simple square network, while the small loops remain empty. Note the checkerboard distribution at $H\ell^2/\phi_0 = 0.02$ corresponding to half filling of the large loops $H(L^2 - \ell^2)/\phi_0 \approx 0.5$.

$H\ell^2/\phi_0 = 0.01$, vortices are located far away from each other; at $H\ell^2/\phi_0 = 0.02$ corresponding to half filling of the large loops $H(L^2 - \ell^2)/\phi_0 \approx 0.5$, a checkerboard distribution[3,12,14] is observed in the large loops, while all small loops are empty; however, at $H\ell^2/\phi_0 = 0.03$ most of the large loops are occupied with one vortex. The small loops, however, are

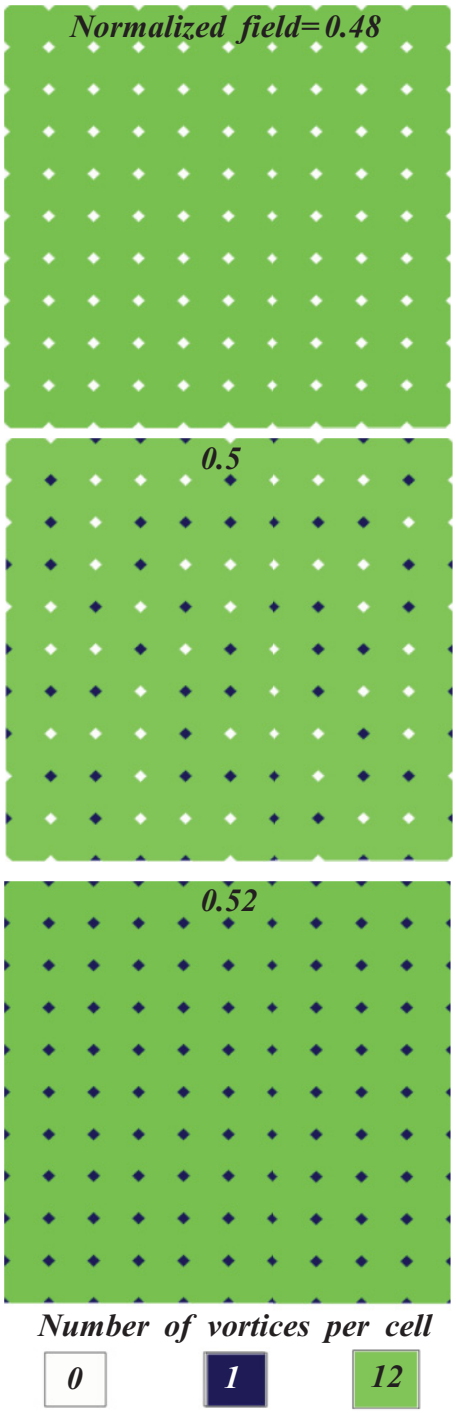

FIG. 6. (Color online) Vortex configuration in the double network at relatively high fields, $H\ell^2/\phi_0 = 0.48,0.5$, and 0.52 for $L/\ell = 5$. Note that in this narrow field range the number of vortices in the small loops increases sharply from zero to one.

empty at all these fields and, therefore, a plateau in $n_v(H)$ is observed in Fig. 4(b).

Figure 6 shows the vortex distribution in a double network with $L/\ell = 5$ at relatively high fields of $H\ell^2/\phi_0 = 0.48,0.50$, and 0.52. In this narrow field range the number of vortices in the small loops increases sharply from zero at 0.48 to one at 0.52. The $n_v(H)$ curve at these fields [Fig. 4(b)] corresponds to the transition from one plateau to another. As the field is further increased the number of vortices in the large loops increases linearly while the number of vortices in the small loops remains constant.

IV. SUMMARY

We have theoretically studied the recently realized superconducting double network consisting of two interlaced subnetworks of small and large loops. Our numerical simulations show that the vortex occupation of the large and small loops is completely different. Vortices prefer to occupy the large loops, even in large numbers, before the occupation of the small loops begins. The population of the subnetwork of the large loops increases linearly with the field, while the occupation of the subnetwork of the small loops grows in steps. The energies of both subnetworks oscillate with the field with different periodicities determined by the areas of the large and small loops. The energy oscillations of the subnetwork of the large loops are of low amplitude and short period and resemble that of a simple square network, exhibiting cusps at the beginning and at the end of each period. These oscillations are superimposed on the high amplitude and long period energy oscillations of the subnetwork of the small loops, which resemble the energy oscillations of isolated loops exhibiting cusps at the middle of each period. The low amplitude of the energy oscillations of the large loops is a result of the relatively small-screening current induced in the large loops. At the end of the first short period each of the large loops is occupied with one vortex, in the next period with two vortices, etc. In contrast, the subnetwork of the small loops remains empty up to fields of approximately half of the long period, i.e., $\phi_0/2\ell^2$. Up to this field the screening current in the small loops increases linearly, and consequently the contribution to the energy increases quadratically with the field. Around $\phi_0/2\ell^2$ in a relatively narrow field range defined by the ratio L/ℓ, all the small loops are filled with one vortex. In the next long period at $3\phi_0/(2\ell^2)$, each of the small loops is occupied with two vortices, etc. Thus the behavior of the small loops resembles that of a single loop.

The above physical picture is explained by a modified mean-field analysis in which we treat the large loops by mean-field interactions and the small loops as disconnected. This hybrid framework yields the stepwise population and energy oscillations in excellent agreement with the numerical simulations. We therefore conclude that the subnetwork of the small loops behaves as a large ensemble of decoupled loops. As demonstrated in Fig. 4(b), the degree of decoupling improves as the size ratio L/ℓ between the two networks increases.

The numerical simulations have the advantage in providing the actual vortex distribution in the network as a function of the external field, as demonstrated in Figs. 5 and 6. Experimental imaging of vortex distribution in simple networks of micron-size squares has been previously performed using Hall-probe technique,[28,29] scanning-SQUID microscopy,[30] and Bitter decoration.[31–33] Extension of these works to imaging of vortex distribution in nano-loops of the double network may be realized by exploiting Magnetic Force and SQUID microscopy. This study may lead to novel designs of network and methods of controlling the position of a single vortex, with

implications to future nano-scale superconducting devices. Our work may also be applicable to the recent activity on arrays of single-domain ferromagnetic islands.[34–36]

ACKNOWLEDGMENTS

This work was supported by the Deutsche Forschungsgemein-schaft through the Deutsch Israelische Projektkooperation (DIP), Grant No. 563363. Y.Y. acknowledges support from the Israel Science Foundation. I.S. thanks the Israeli Ministry of Science and Technology for the Eshkol scholarship.

APPENDIX A

1. Kirchoff-law's matrices for the simple square network

The four $M^2 \times M^2$ matrices, K^0,K^1,K^2, and K^3, with periodic boundary conditions have the form

$$K^0_{\alpha\beta} = \begin{cases} 1 & \text{if} \quad \alpha = \beta \\ -1 & \text{if} \quad \alpha = \beta + 1 \text{ and } \alpha \neq 0,\ M,\ 2M \ldots M^2 - M \\ -1 & \text{if} \quad \alpha = \beta - M + 1 \text{ and } \alpha = 0,\ M,\ 2M \ldots M^2 - M \\ 0 & \text{otherwise} \end{cases}; \tag{A1}$$

$$K^1_{\alpha\beta} = \begin{cases} 1 & \text{if} \quad \alpha = \beta \\ -1 & \text{if} \quad \alpha = \beta + M \text{ and } \alpha \geqslant M \\ -1 & \text{if} \quad \alpha = \beta - M^2 + M \text{ and } \alpha < M \\ 0 & \text{otherwise} \end{cases}; \tag{A2}$$

$$K^2_{\alpha\beta} = \begin{cases} 1 & \text{if} \quad \alpha = \beta \\ -1 & \text{if} \quad \alpha = \beta - 1 \text{ and } \alpha \neq M - 1,\ 2M - 1 \ldots M^2 - 1 \\ -1 & \text{if} \quad \alpha = \beta + M - 1 \text{ and } \alpha \neq M - 1,\ 2M - 1 \ldots M^2 - 1 \\ 0 & \text{otherwise} \end{cases}; \tag{A3}$$

$$K^3_{\alpha\beta} = \begin{cases} 1 & \text{if} \quad \alpha = \beta \\ -1 & \text{if} \quad \alpha = \beta - M \text{ and } \alpha < M^2 - M \\ -1 & \text{if} \quad \alpha = \beta + M^2 - M \text{ and } \alpha \geqslant M^2 - M \\ 0 & \text{otherwise} \end{cases}. \tag{A4}$$

These matrices use Kirchoff's law to express the total current in a specific wire in a square network using the circular currents in two adjacent loops sharing the same wire, using Eq. (11) one can get, for example, $J_{0,M+1} = \tilde{J}_{M+1} - \tilde{J}_M$, $J_{1,M+1} = \tilde{J}_{M+1} - \tilde{J}_1$, $J_{1,M+1} = \tilde{J}_{M+1} - \tilde{J}_{M+2}$, and $J_{1,M+1} = \tilde{J}_{M+1} - \tilde{J}_{2M+1}$.

APPENDIX B

1. Kirchoff-law's matrices for the double network

The matrices A^δ, B^δ,C^γ, and D^γ with periodic boundary condition are evaluated as

$$\begin{gathered} A^1_{\alpha\beta} = K^0_{\alpha\beta}; \quad A^3_{\alpha\beta} = K^1_{\alpha\beta}; A^5_{\alpha\beta} = K^2_{\alpha\beta}; \quad A^7_{\alpha\beta} = K^3_{\alpha\beta}; \\ A^0_{\alpha\beta} = A^2_{\alpha\beta} = A^4_{\alpha\beta} = A^6_{\alpha\beta} = \begin{cases} 1 & \text{if} \quad \alpha = \beta \\ 0 & \text{otherwise} \end{cases}; \end{gathered} \tag{B1}$$

$$B^1_{\alpha\beta} = B^3_{\alpha\beta} = B^5_{\alpha\beta} = B^7_{\alpha\beta} = 0;$$

$$B^0_{\alpha\beta} = \begin{cases} -1 & \text{if} \quad \alpha = \beta - M \text{ and } \alpha < M^2 - M \\ -1 & \text{if} \quad \alpha = \beta + M^2 - M \text{ and } \alpha \geqslant M^2 - M \\ 0 & \text{otherwise} \end{cases};$$

$$B^2_{\alpha\beta} = \begin{cases} -1 & \text{if} \quad \alpha = \beta \\ 0 & \text{otherwise} \end{cases};$$

$$B^4_{\alpha\beta} = \begin{cases} -1 & \text{if} \quad \alpha = \beta - 1 \text{ and } \alpha \neq M - 1,\ 2M - 1 \ldots M^2 - 1 \\ -1 & \text{if} \quad \alpha = \beta + M - 1 \text{ and } \alpha = M - 1,\ 2M - 1 \ldots M^2 - 1 \\ 0 & \text{otherwise} \end{cases};$$

$$B^6_{\alpha\beta} = \begin{cases} 0 & \text{if} \quad \alpha = M^2 - 1 \text{ and } \beta = 0 \\ -1 & \text{if} \quad \alpha = \beta - M - 1 \text{ and } \alpha < M^2 - M \text{ and } \alpha \neq M - 1,\ 2M - 1 \ldots M^2 - M - 1 \\ -1 & \text{if} \quad \alpha = \beta - 1 \text{ and } \alpha = M - 1,\ 2M - 1 \ldots M^2 - M - 1 \\ -1 & \text{if} \quad \alpha = \beta + M^2 - M - 1 \text{ and } \alpha \neq M^2 - 1 \text{ and } \alpha \neq M - 1,\ 2M - 1 \ldots M^2 - M - 1 \\ 0 & \text{otherwise} \end{cases};$$

$$C^0_{\alpha\beta} = \begin{cases} 0 & \text{if} \quad \alpha = 0 \text{ and } \beta = M^2 - 1 \\ -1 & \text{if} \quad \alpha = \beta - M^2 + M + 1 \text{ and } 0 < \alpha < M \\ -1 & \text{if} \quad \alpha = \beta + 1 \text{ and } \alpha = M, 2M \ldots M^2 - M \text{ and } \alpha \neq 0 \\ -1 & \text{if} \quad \alpha = \beta + M + 1 \text{ and } \alpha > M - 1 \text{ and } \alpha \neq M, 2M \ldots M^2 - M \\ 0 & \text{otherwise} \end{cases};$$

$$C^1_{\alpha\beta} = \begin{cases} -1 & \text{if} \quad \alpha = \beta - M^2 + M \text{ and } \alpha < M \\ -1 & \text{if} \quad \alpha = \beta + M \text{ and } \alpha \geqslant M \\ 0 & \text{otherwise} \end{cases}; \tag{B2}$$

$$C^2_{\alpha\beta} = \begin{cases} -1 & \text{if} \quad \alpha = \beta \\ 0 & \text{otherwise} \end{cases};$$

$$C^3_{\alpha\beta} = \begin{cases} -1 & \text{if} \quad \alpha = \beta - M + 1 \text{ and } \alpha = 0, M \ldots M^2 - M \\ -1 & \text{if} \quad \alpha = \beta + 1 \text{ and } \alpha \neq \alpha = 0, M \ldots M^2 - M \\ 0 & \text{otherwise} \end{cases};$$

$$D^0_{\alpha\beta} = D^1_{\alpha\beta} = D^2_{\alpha\beta} = D^3_{\alpha\beta} = \begin{cases} 1 & \text{if} \quad \alpha = \beta \\ 0 & \text{otherwise} \end{cases}. \tag{B3}$$

These matrices use Kirchoff's law to express the total current in a specific wire in the double network using the circular currents in two adjacent loops sharing the same wire. Using Eq. (27) one can get, for example, $J_{1,M+1} = \tilde{J}_{M+1} - \tilde{J}_M$ and $j_{2,M+1} = \tilde{j}_{M+1} - \tilde{J}_{M+1}$.

[1] F. London, Phys. Rev. **74**, 562 (1948).
[2] W. A. Little and R. D. Parks, Phys. Rev. Lett. **9**, 9 (1962).
[3] An extensive literature on low-T_c superconducting networks can be found in Proceedings of the NATO Workshop on Conference in Superconducting Networks, Delft, The Netherlands, 1987, edited by J. E. Mooij and G. Schon [Physica B **152**, Issues 1-2 (1988)].
[4] S. Alexander, Phys. Rev. B **27**, 1541 (1983).
[5] P. G. de Gennes, C. R. Acad. Sci. Ser. B **292**, 9 (1981).
[6] P. G. de Gennes, C. R. Acad. Sci. Ser. B **292**, 279 (1981).
[7] H. J. Fink, A. Lopez, and R. Maynard, Phys. Rev. B **26**, 5237 (1982).
[8] B. Pannetier, J. Chaussy, and R. Rammal, J. Phys. (Paris) Lett. **44**, 853 (1983).
[9] B. Pannetier, J. Chaussy, R. Rammal, and J. C. Villegier, Phys. Rev. Lett. **53**, 1845 (1984).
[10] R. Rammal, T. C. Lubensky, and G. Toulouse, Phys. Rev. B **27**, 2820 (1983).
[11] J. Simonin, D. Rodrigues, and A. Lopez, Phys. Rev. Lett. **49**, 944 (1982).
[12] A. Behrooz, M. J. Burns, D. Levine, B. Whitehead, and P. M. Chaikin, Phys. Rev. B **35**, 8396 (1987).
[13] P. M. Chaikin, A. Behrooz, M. A. Itzler, C. Wilks, B. Whitehead, G. Grest, and D. Levine, Physica B **152**, 113 (1988).
[14] M. A. Itzler, A. M. Behrooz, C. W. Wilks, R. Bojko, and P. M. Chaikin, Phys. Rev. B **42**, 8319 (1990).
[15] H. Yoshino, T. Nogawa, and B. Kim, New J. Phys. **11**, 013010 (2009).
[16] E. Granato, Phys. Rev. Lett. **101**, 027004 (2008).
[17] S. J. Lee, B. Kim, and J. Lee, Physica A **315**, 314 (2002).
[18] I. Sochnikov, A. Shaulov, Y. Yeshurun, G. Logvenov, and I. Bozovic, Nature Nanotech. **5**, 516 (2010).
[19] I. Sochnikov, A. Shaulov, Y. Yeshurun, G. Logvenov, and I. Bozovic, Phys. Rev. B **82**, 094513 (2010).
[20] C. Reichhardt, C. J. Olson Reichhardt, and A. R. Bishop, Physica C **460**, 1178 (2007).
[21] M. Tinkham, *Introduction to Superconductivity* (McGraw-Hill, New York, 1996), pp. 127–129.
[22] V. G. Kogan, J. R. Clem, and R. G. Mints, Phys. Rev. B **69**, 064516 (2004).
[23] E. H. Brandt and J. R. Clem, Phys. Rev. B **69**, 184509 (2004).
[24] S. Teitel and C. Jayaprakash, Phys. Rev. Lett. **51**, 1999 (1983).
[25] T. C. Halsey, Phys. Rev. B **31**, 5728 (1985).
[26] Note that in the analytical solution, due to its mean-field nature, we require that the average current in the network vanishes, while in the numerical simulations we require current conservation at every node.
[27] The breaks around the middle of the steps result from competition in occupation of large and small loops. This competition occurs in the field range where the energy cost to insert a vortex into a small loop or a large loop is similar.
[28] A. M. Chang, H. D. Hallen, L. Harriott, H. F. Hess, H. L. Kao, J. Kwo, R. E. Miller, R. Wolfe, J. van der Ziel, and T. Y. Chang, Appl. Phys. Lett. **61**, 1974 (1992).
[29] H. D. Hallen, R. Seshadri, A. M. Chang, R. E. Miller, L. N. Pfeiffer, K. W. West, C. A. Murray, and H. F. Hess, Phys. Rev. Lett. **71**, 3007 (1993).

[30]L. N. Vu, M. S. Wistrom, and D. J. Van Harlingen, Appl. Phys. Lett. **63**, 1693 (1993).
[31]K. Runge and B. Pannetier, Europhys. Lett. **24**, 737 (1993).
[32]E. Serret, P. Butaud, and B. Pannetier, Europhys. Lett. **59**, 225 (2002).
[33]A. Bezryadin, Y. N. Ovchinnikov, and B. Pannetier, Phys. Rev. B **53**, 8553 (1996).
[34]C. Nisoli, J. Li, X. Ke, D. Garand, P. Schiffer, and V. H. Crespi, Phys. Rev. Lett. **105**, 047205 (2010).
[35]C. Nisoli, R. Wang, J. Li, W. F. McConville, P. E. Lammert, P. Schiffer, and V. H. Crespi, Phys. Rev. Lett. **98**, 217203 (2007).
[36]R. F. Wang, C. Nisoli, R. S. Freitas, J. Li, W. McConville, B. J. Cooley, M. S. Lund, N. Samarth, C. Leighton, V. H. Crespi, and P. Schiffer, Nature (London) **439**, 303 (2006).